Inviscid Flow Through Converging-Diverging Nozzle

SmartNumerics Simulation Solutions Inc.

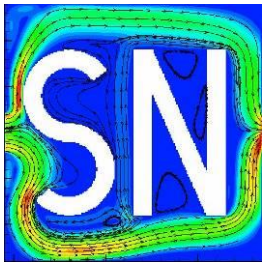

June 5, 2020

Table of Contents

1.0 Introduction

A useful verification nozzle test case involving inviscid flow is provided by the NPARC Alliance at http://www.grc.nasa.gov/WWW/wind/valid/cdv/cdv.html. This page contains a link to test results produced by the Wind CFD code. The nozzle cross-sectional area has the form

$$A = \begin{cases} 1.75 - 0.75\cos\left((0.2x - 1)\pi\right) & \text{for} \quad 0 \le x \le 5 \\ 1.25 - 0.25\cos\left((0.2x - 1)\pi\right) & \text{for} \quad 5 \le x \le 10 \end{cases}$$

The plenum (reservoir) total pressure and temperature are 1 PSI and 100° Rankine, respectively. Numerical results and analytical solutions are provided for exit static pressures of 0.89, 0.75, and 0.16 PSI, which correspond to subsonic outflow with isentropic flow, subsonic outflow with normal shock in diffusing section, and supersonic outflow with isentropic flow, respectively. The conservation of mass can be evaluated. The constancy of total pressure in a duct without shocks (isentropic) can be determined.

Figure 1 display plays the initial grid and parameters for the converging-diverging nozzle. The inflow condition on the west edge of the grid imposes total pressure and total temperature. The outflow condition on the east imposes a static pressure of 0.89, 0.75, or 0.16 PSI. A symmetry condition is imposed at the south edge of the grid which is located at the axis of the nozzle. A slip boundary condition is imposed at the north edge. The initial state consists of Mach 0.99 flow with a total pressure of 1 PSI and a total temperature of 100 degrees Rankine.

The simulation was performed using a five-stage explicit Runge-Kutta algorithm using a CFL of 0.45 per stage. The HLLC flux was used with the van Albada limiter. Convergence to the steady state was enhanced using application of fourth-order dissipation, implicit residual smoothing, and enriched w-cycle multigrid (4 subgrids). The solution after 1000 cycles was transferred to a grid with four times the number of cells and run for an additional 1000 cycles. This solution was transferred to an even finer grid and run for an additional 1500 cycles.

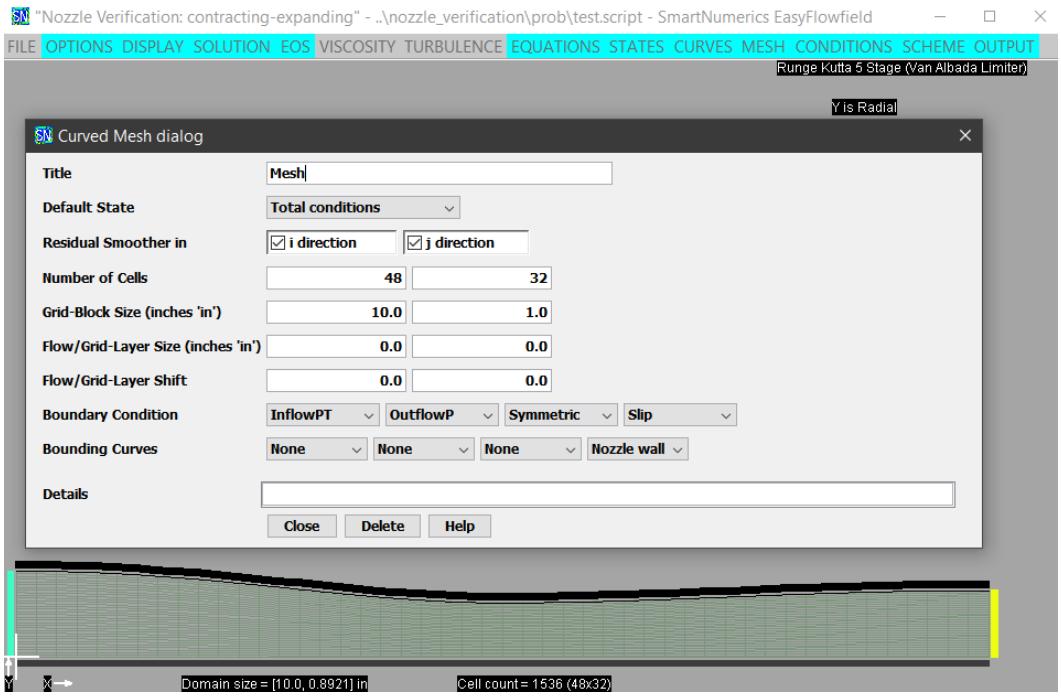

Fig. 1: Initial grid for converging-diverging nozzle.

2.0 Solution for Exit Pressure of 0.89 PSI

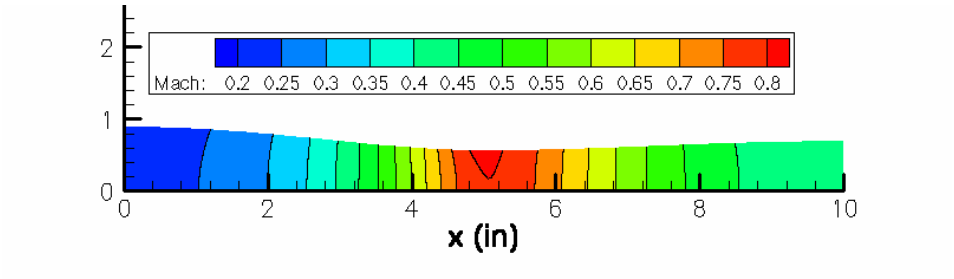

Fig. 2a: Mach contours on finest grid with exit pressure set to 0.89 PSI.

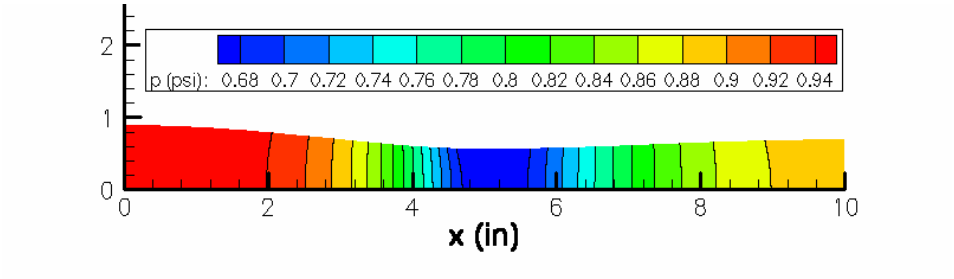

Fig. 2b: Pressure contours on finest grid with exit pressure set to 0.89 PSI.

Figures 2a and 2b display contours of Mach number and pressure on the final 192x128 cell grid with exit pressure set to 0.89 PSI. Flow speed is highest, and pressure is lowest in the throat of the nozzle.

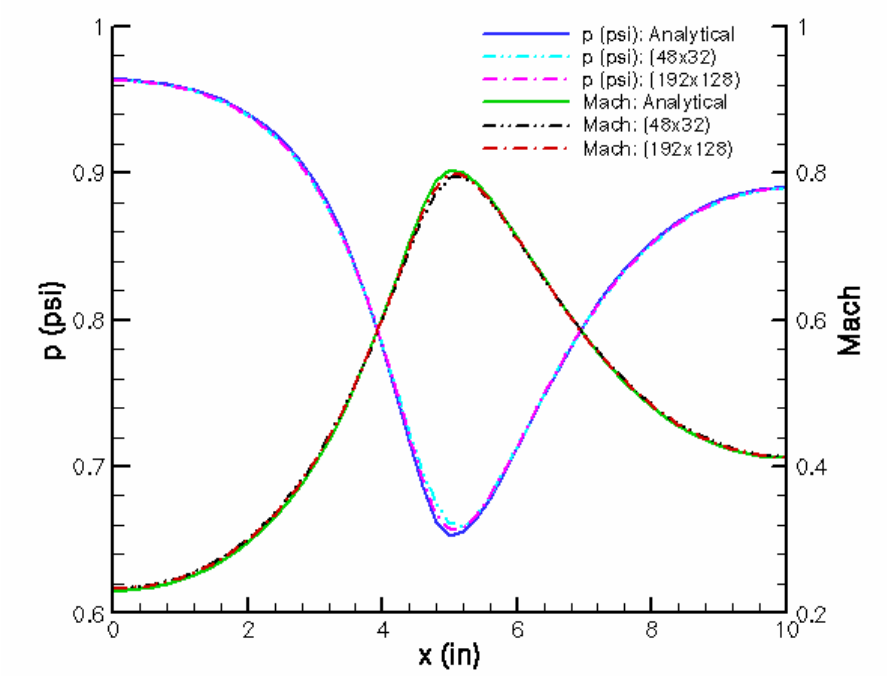

Fig. 2c: Mach number and pressure along nozzle axis for exit pressure of 0.89 PSI.

Figure 2c compares Mach number and pressure along the axis of the nozzle to the analytical reference curves. As expected, the solution from the finest grid gives the best match to the reference curves.

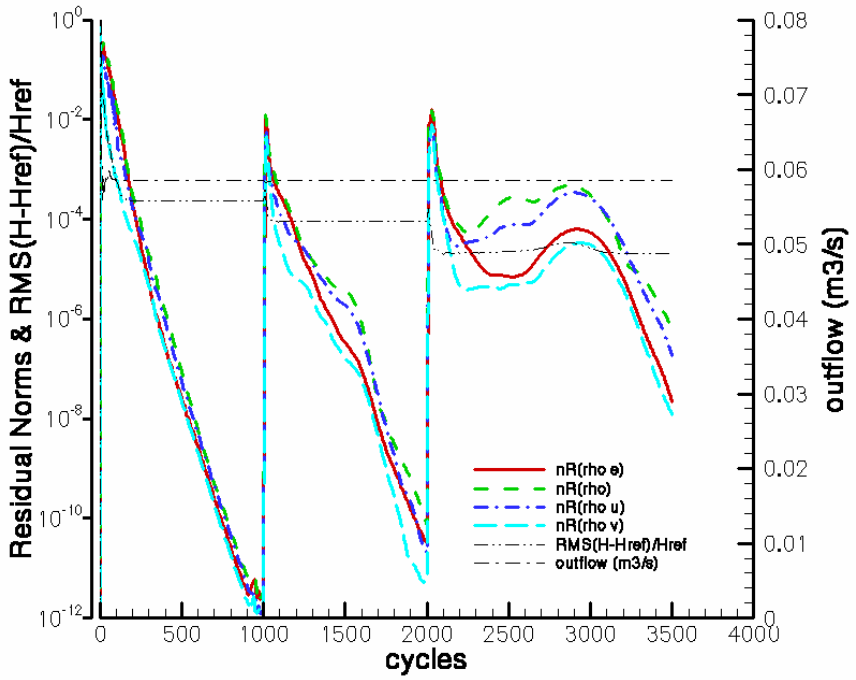

Fig. 2d: Convergence history with exit pressure set to 0.89 PSI.

Figure 2d displays the convergence history with the exit pressure set to 0.89 PSI. The normalized residuals of energy, density, and momentum decrease in a similar way with the number of cycles on each grid except for the finest grid where some hesitation is encountered. The volumetric rate at the exit reaches a constant

value early in the simulation. For inviscid flow, the total enthalpy, *H*, in each cell should approach the inflow total enthalpy. The corresponding Root Mean Square average measure, RMS(H-Href)/Href, is closest to zero on the finest grid which has the smallest dissipation.

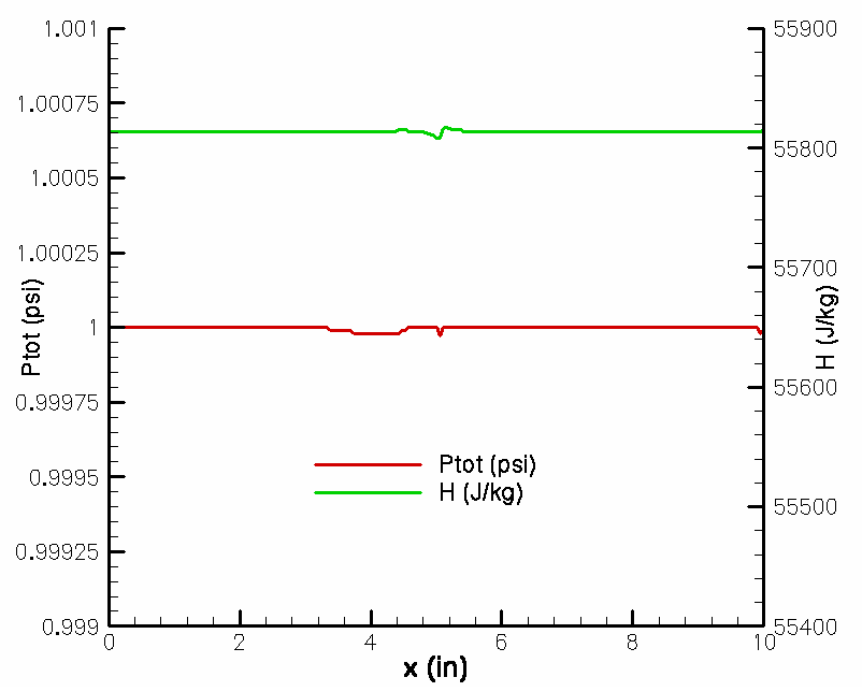

Fig. 2e: Total pressure and total enthalpy along axis on finest grid (P_{exit} = 0.89 PSI).

As seen in Figure 2e, the total pressure and total enthalpy are respectively constant within 0.02% and 0.04%.

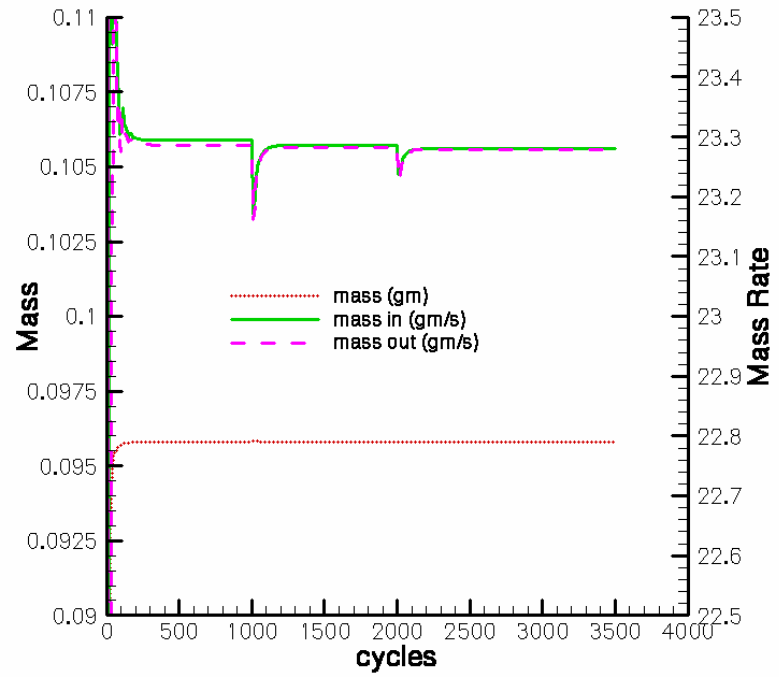

Fig. 2f: Conservation history for nozzle with exit pressure set to 0.89 PSI.

As seen in Figure 2f, the rate of mass outflow approaches the rate of the mass inflow ever more closely as the grid is refined. Geometrical source terms used to impose the cylindrical symmetry produce the small mismatch.

3.0 Solution for Exit Pressure of 0.75 PSI

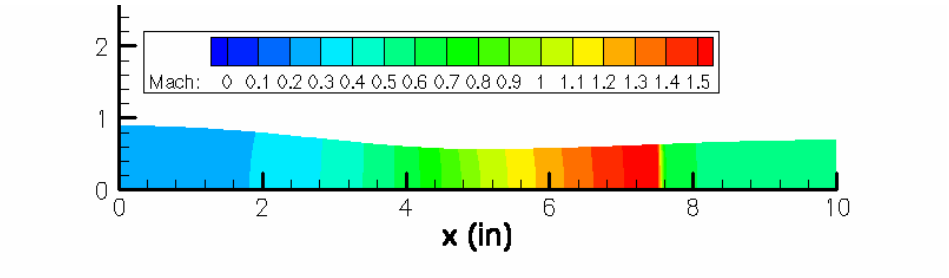

Fig. 3a: Mach number contours on finest grid with exit pressure set to 0.75 PSI.

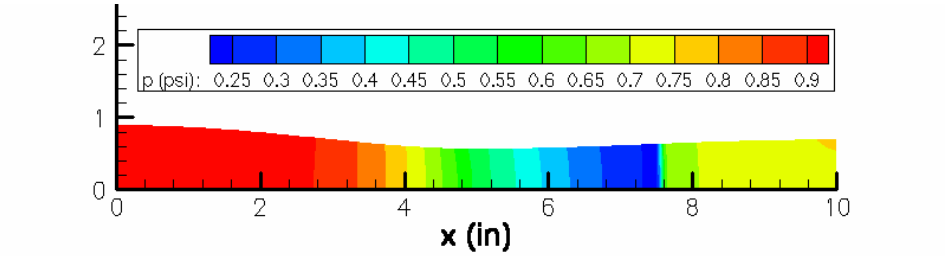

Fig. 3b: Pressure contours on finest grid with exit pressure set to 0.75 PSI.

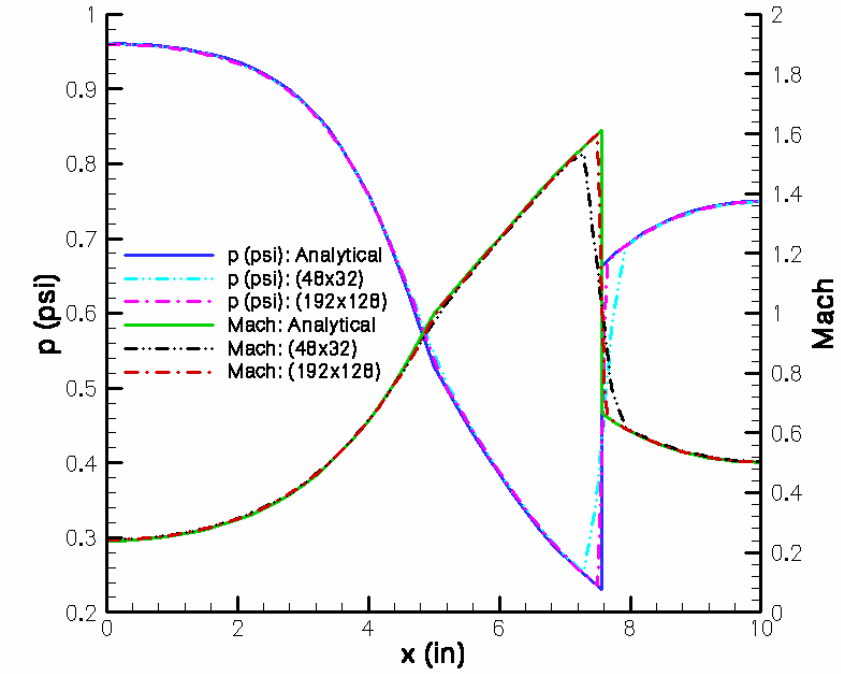

Fig. 3c: Mach number and pressure along nozzle axis for exit pressure of 0.75 PSI.

Figures 3a and 3b display contours of Mach number and pressure on the final 192x128 cell grid with exit pressure set to 0.75 PSI. The flow speed gradually rises in the streamwise direction until it reaches the speed of sound at the nozzle throat and continues to increase until it abruptly decreases to a subsonic value at the upstream-facing stationary shock and continues to gradually decrease downstream of the shock.. Pressure gradually decreases in the stream-wise direction until it abruptly increases at the stationary shock and continues to gradually increase downstream of the shock. This can be seen more clearly in Figure 3c which also displays the solution from the initial grid.

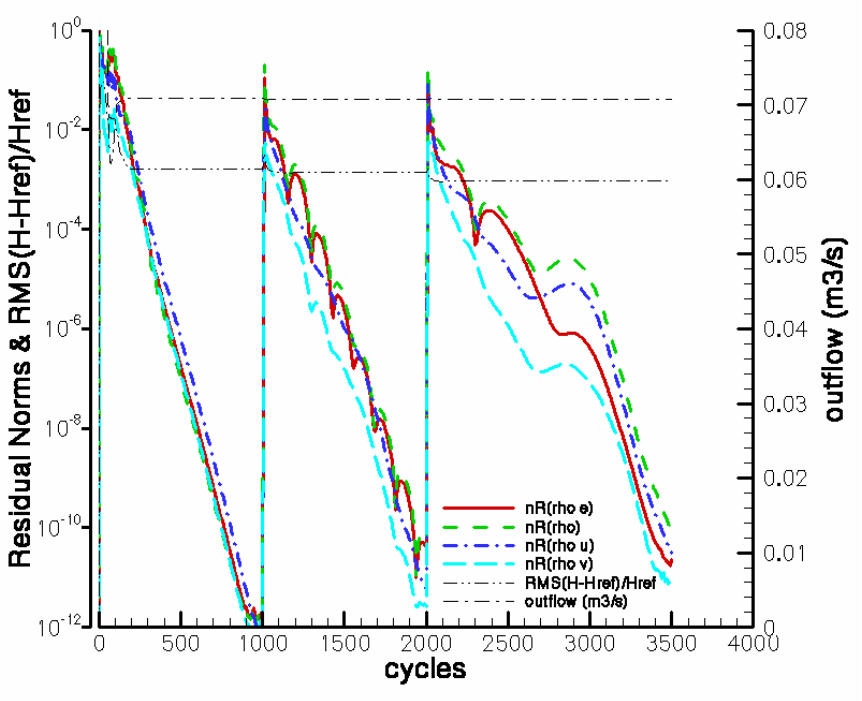

Fig. 3d: Convergence history with exit pressure set to 0.75 PSI.

In Figure 3d there is a larger RMS average departure from the inflow value of total enthalpy than seen with an exit pressure of 0.89 PSI. As seen in Figure 3e, the total enthalpy is constant within 0.04% except for spike at the location of the shock which produces the larger RMS average departure from the inflow value of total enthalpy. The total pressure is constant upstream of the shock except for small disturbances. There is a spike at the shock then the total pressure remains constant at a lower value owing to the total pressure loss produced by non-isentropic compression at the shock.

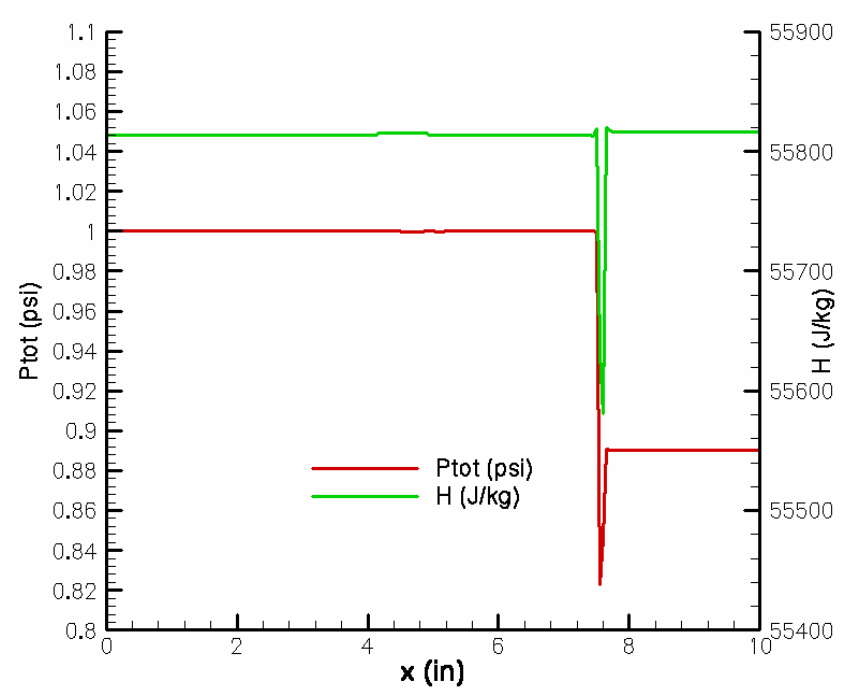

Fig. 3e: Total pressure and total enthalpy along axis on finest grid (P_{exit} = 0.75 PSI).

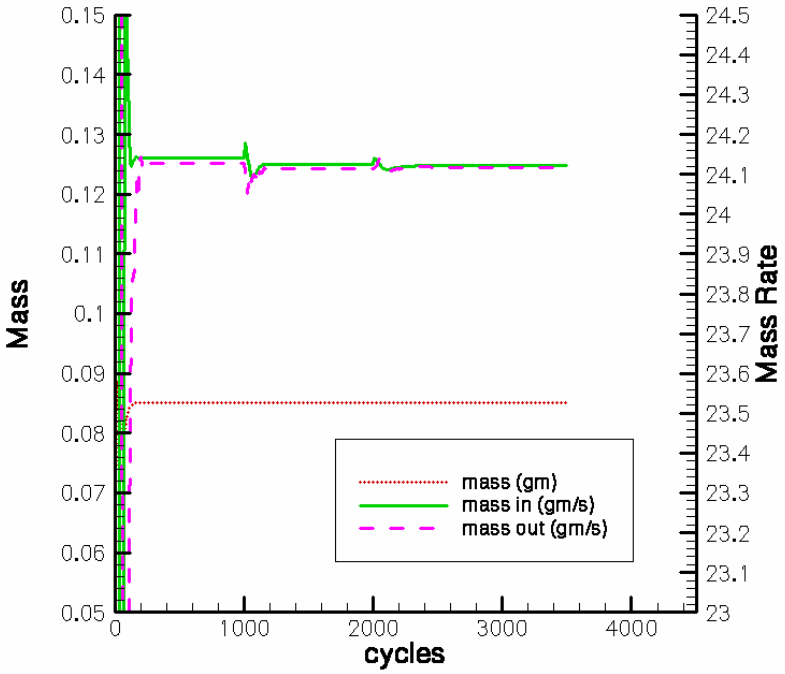

Fig. 3f: Conservation history for nozzle with exit pressure set to 0.75 PSI.

4.0 Solution for Exit Pressure of 0.16 PSI

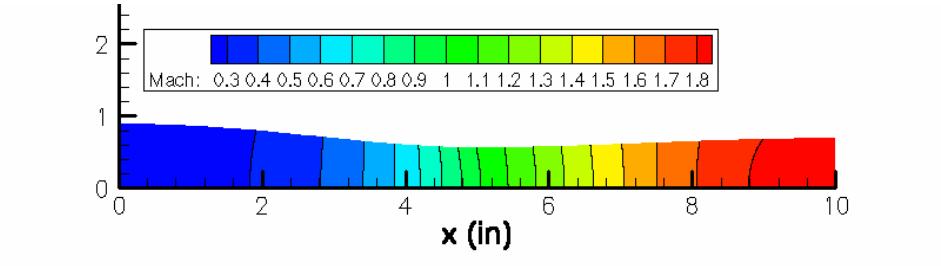

Fig. 4a: Mach number contours on finest grid with exit pressure set to 0.16 PSI.

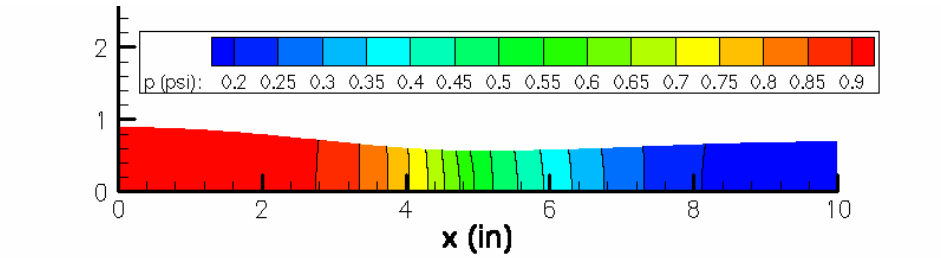

Fig. 4b: Pressure contours on finest grid with exit pressure set to 0.16 PSI.

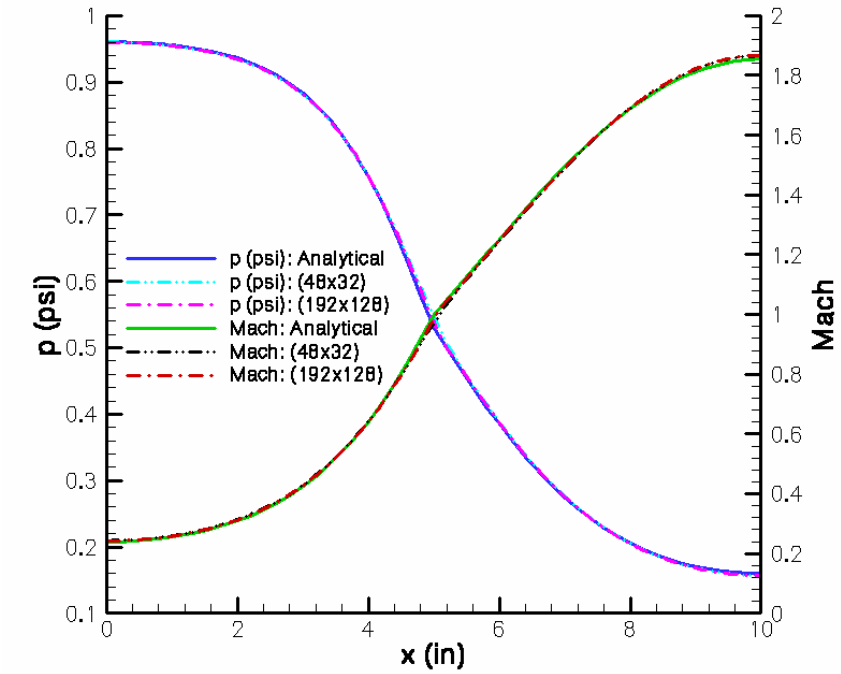

Fig. 4c: Mach number and pressure along nozzle axis for exit pressure of 0.15 PSI.

Figures 3a and 3b display contours of Mach number and pressure on the final 192x128 cell grid with exit pressure set to 0.16 PSI. The flow speed gradually rises in the stream-wise direction until it reaches the speed of sound at nozzle throat and continues to increase until the exit. The pressure gradually decreases in the stream-wise direction until the exit is reached. This can be seen more clearly in Figure 4c which also displays the solution from the initial grid.

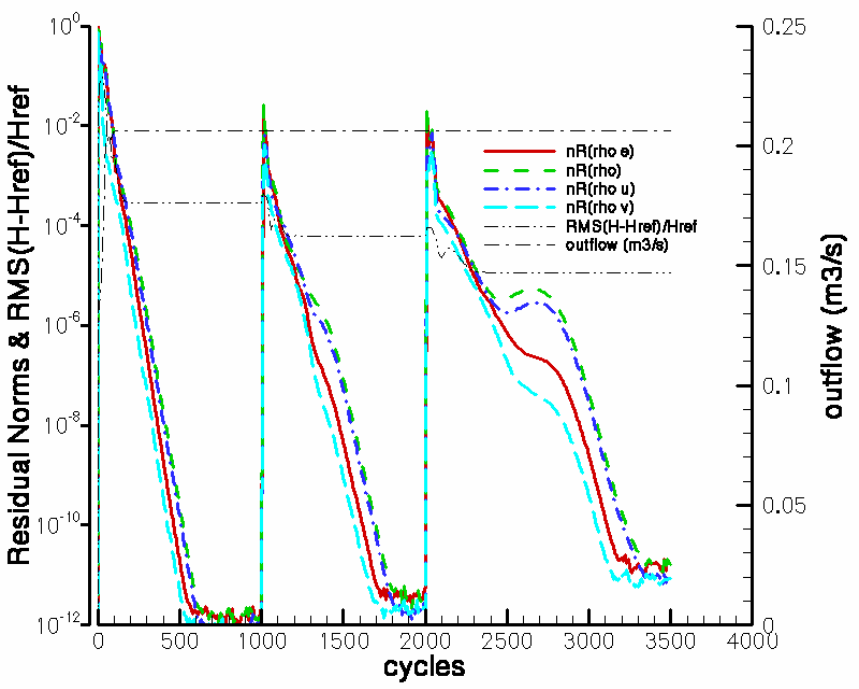

Fig. 4d: Convergence history with exit pressure set to 0.16 PSI.

In Figure 4d the RMS average departure from the inflow value of total enthalpy is similar to that seen with an exit pressure of 0.89 PSI. As seen in Figure 4e, the total pressure and total enthalpy are respectively constant within 0.05% and 0.04%, with most variation occurring near the throat and exit.

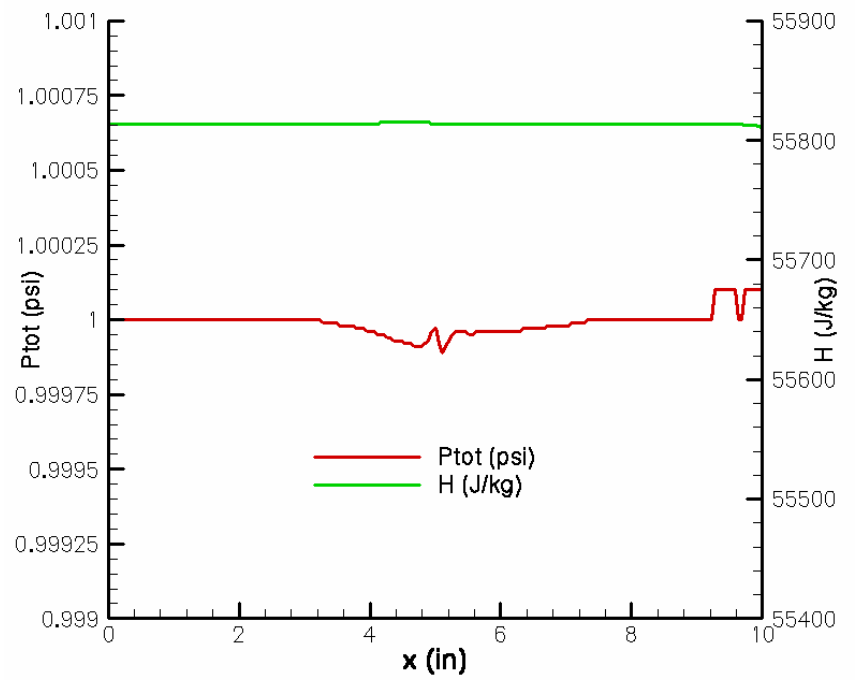

Fig. 4e: Total pressure and total enthalpy along axis on finest grid (P_{exit} = 0.16 PSI).

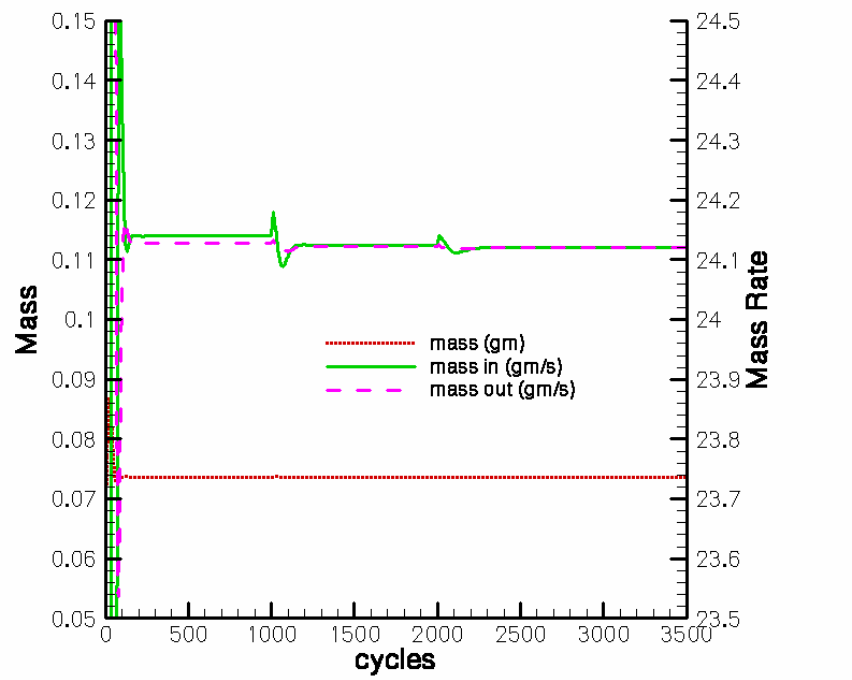

Fig. 4f: Conservation history for nozzle with exit pressure set to 0.16 PSI.